Sensors and Materials, Vol. 36, No. 1 (2024) 169–176
MYU Tokyo

S & M 3507

Temperature Dependence of α-Particle Detection Performance of GaN PIN Diode Detector

Hisaya Nakagawa,[1] Kosuke Hayashi,[2] Atsuya Miyazawa,[2] Yoshio Honda,[3] Hiroshi Amano,[3] Toru Aoki,[1] and Takayuki Nakano[1,2*]

[1]Research Institute of Electronics, Shizuoka University, 3-5-1 Johoku, Chuo-ku, Hamamatsu 432-8011, Japan
[2]Department of Electronics and Materials Science, Shizuoka University, 3-5-1 Johoku, Chuo-ku, Hamamatsu, 432-8561 Japan
[3]Institute of Materials and Systems for Sustainability, Nagoya University, Furo-cho, Chikusa-ku, Nagoya 464-8601, Japan

(Received September 6, 2023; accepted January 18, 2024)

Keywords: GaN detector, high-temperature tolerance, semiconductor detector, radiation detector, PIN diodes

Group-III nitride semiconductors, such as gallium nitride (GaN), have been proposed as novel materials for radiation detection owing to their wide bandgap and their ability to operate at high temperatures. In this study, the radiation detection properties of GaN PIN diode detectors were evaluated at high temperatures (~573 K). The energy spectrum peak profiles of ^{241}Am α-particles were obtained at different temperatures, confirming the operation of GaN PIN diodes up to 573 K. The peak positions shifted toward the lower-energy side and the full width at half maximum (FWHM) of the detection energy peak improved with increasing temperature. Furthermore, the variation in electron carrier mobility–lifetime product ($\mu_e\tau_e$) between 293 and 573 K was not significant. These results indicate the potential high-temperature operation of group-III nitride semiconductors. Additionally, the variation in each detection characteristic was caused by increasing the atmospheric temperature, which affected the mobility, lattice scattering, bandgap, and built-in potential differently.

1. Introduction

Gallium nitride (GaN) semiconductors have broad applications in blue LEDs[1,2] and power transistors.[3,4] GaN has numerous attractive properties, such as a wide bandgap and high thermal stability, which render it suitable for radiation detection at room temperature. Various materials have been studied as promising radiation detectors, including silicon (Si),[5–7] cadmium telluride (CdTe),[8–10] cadmium zinc telluride (CZT),[11,12] silicon carbide (SiC),[13,14] thallium bromide (TlBr),[15–17] and GaN.[18,19]

BGaN, an alloy crystal containing BN and GaN, has recently been proposed as a neutron detector semiconductor.[20–23] BGaN neutron detectors are advantageous because the B atom has a large neutron capture cross-sectional area. Owing to the existence of atomic-level B convertors

*Corresponding author: e-mail: nakano.takayuki@shizuoka.ac.jp
https://doi.org/10.18494/SAM4647

ISSN 0914-4935
https://myukk.org/

in semiconductors, BGaN can detect the energy of generated-charged particles using the ^{10}B (n, a) ^{7}Li neutron capture reaction. Additionally, BGaN exhibits low γ-ray sensitivity owing to its small atomic mass.[20,22] These properties indicate that BGaN can be used as a neutron detector with high neutron–γ-ray (n/g) discrimination. Furthermore, neutron detection using a vertical BGaN PIN diode detector has been reported.[21] Hence, neutron detectors based on group-III nitride semiconductors have potential applicability.

Owing to their low thermal noise, wide-bandgap semiconductor radiation detectors do not require a cooling system. Therefore, wide-bandgap semiconductors facilitate high-temperature operation without a cooling system, enabling the realization of miniaturized detection devices with reduced size, power consumption, and cost. Wide-bandgap semiconductor detectors using SiC[24] and diamond[25] have been developed as γ-ray detectors for operation at high temperatures. However, a BGaN semiconductor, which is used as a neutron detector unlike SiC and diamond but is similar to wide-bandgap semiconductors such as SiC and diamond, requires further investigation of its radiation detection characteristics at high temperatures. Reportedly, GaN high-electron-mobility transistors (HEMTs) are stable at high temperatures (~673 K).[26,27] For neutron detection in the nuclear instrumentation of nuclear power plants, a neutron detector that can operate in high-temperature environments is useful.[28] Therefore, a BGaN neutron detector using a wide-bandgap semiconductor material has potential use as a novel nuclear instrument.

To this end, the thermal tolerance of group-III nitride detectors requires investigation. Therefore, in this study, we evaluated the radiation detection characteristics of GaN PIN diode detectors at high temperatures and verified the thermal tolerance of GaN, which is the base material for BGaN. Furthermore, GaN PIN diode detectors were irradiated with ^{241}Am α-particles at temperatures ranging from 293 to 573 K, and their energy spectra were analyzed. Finally, the energy spectra peak profiles of ^{241}Am α-particles were observed at each temperature, confirming that GaN PIN diode detectors can operate at temperatures up to 573 K.

2. Experimental Methods

GaN PIN diodes were fabricated on an a-Al_2O_3 substrate by metal-organic vapor phase epitaxy (MOVPE). The p-GaN/i-GaN/n-GaN structure on the substrate comprised a Mg-doped p-GaN layer of 0.2 mm thickness, an undoped i-GaN layer of 1 mm thickness, and a Si-doped n-GaN layer of 1 mm thickness. Furthermore, Au/Ni and Au/Ti/Al/Ti electrodes were used for p-GaN and n-GaN, respectively. The configurations of the GaN diode and electrode structure are described in Ref. 21, wherein the undoped i-GaN layer acted as a sensitive layer for α-particle detection.

To investigate its radiation detection characteristics, the fabricated GaN PIN diode detector was subjected to a reverse bias voltage of −3 V and irradiated with α-particles from an ^{241}Am radioisotope (RI), which is an RI source sealed with a Au film of about 1 μm. The detector was connected to a charge-sensitive amplifier (ANSeeN Inc., ANS-CSAPA100-01-SN) using a mineral-insulated (MI) cable, and the amplifier's output pulse signals were analyzed using a multichannel analyzer (ANSeeN Inc., ANS-HSDMCA4M4N17) that simultaneously measures

their detected energy and rise time. The ^{241}Am RI was placed at a distance of 19 mm from the detector (incident energy to the GaN PIN detector of approximately 2.3 MeV after air attenuation calculated using the Monte Carlo simulation code PHITS ver.3.08.[29]). The temperature was increased from 293 K (room temperature) to 573 K by heating the shield box containing the detector by using a hot plate. The maximum setting temperature of the hot plate was 673 K, and the substrate surface temperature at that time was 573 K.

3. Results and Discussion

The α-particle energy spectrum of the GaN PIN diode detector was measured at each temperature (293, 323, 373, 423, 473, 523, and 573 K). Figure 1 shows the 2D energy spectrum at each temperature. A 2D histogram was used to analyze the variations in peak value and rise time owing to the increase in temperature.

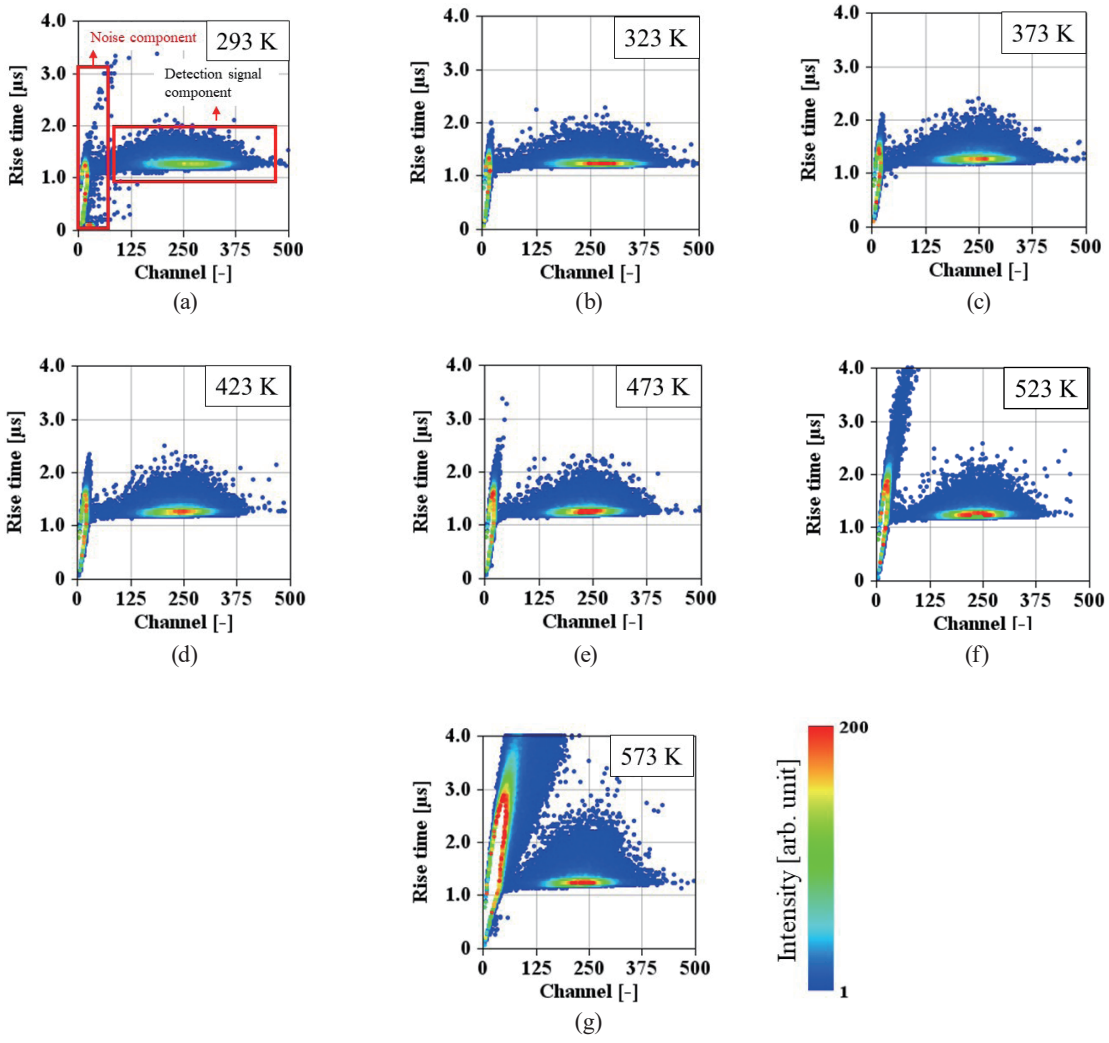

Fig. 1. (Color online) Two-dimensional histograms of the energy and rise time of α-particle detection at (a) 293, (b) 323, (c) 373, (d) 423, (e) 473, (f) 523, and (g) 573 K.

As shown in Fig. 1(a), the noise and α-particle detection signal components at room temperature correspond to the energy channel signals containing fewer and greater than 70 energy channels, respectively. The α-particle detection signal components were obtained at temperatures below 573 K. Furthermore, the region of noise components and, consequently, the thermal noise signals increased with temperature. The α-particle detection signal and noise components exist near 125 ch at 573 K, as shown in Fig. 1(g). Therefore, a technique is required to distinguish the detection signal and noise components at high temperatures.

Figure 2(a) shows a rise-time histogram over the energy channel of 125 ch at 573 K, confirming that this tendency was different at a rise time of approximately 2.5 ms, corresponding to the boundary between the detection and noise signals. Therefore, a rise time of 2.5 ms was defined as the threshold, and the α-particle energy spectra were plotted at and below this value, as shown in Fig. 2(b). The α-particle detection components at 523 and 573 K in Figs. 1(f) and 1(g), respectively, existed in the region above the threshold rise time. However, given the significantly low count of detection signals observed over a rise time of 2.5 μs at 573 K, as depicted in Fig. 2(b), it is feasible to distinguish noise components using data collected under the same rise time. Hence, the detection signal and noise components can be distinguished using the threshold rise time.

Figure 3(a) shows α-particle energy spectra plotted using values under the threshold rise time, wherein the α-particle peak profiles were detected at each temperature. Furthermore, Fig. 3(b) shows the peak position and full width at half maximum (FWHM) values obtained using Fig. 3(a). With increasing temperature, the peak position of the detection energy spectra shifts toward a slightly lower energy channel. This result indicates that the detected signal pulse intensity decreased with rising temperature, meaning that the number of electron–hole pairs generated by an α-particle is decreasing. The path length of the 2.3 MeV α-particle in GaN is approximately 5 mm, which is greater than the sensitive layer thickness. Therefore, the shrinkage of the bandgap and electron–hole pair creation energy with increasing temperature leads to a shift of the

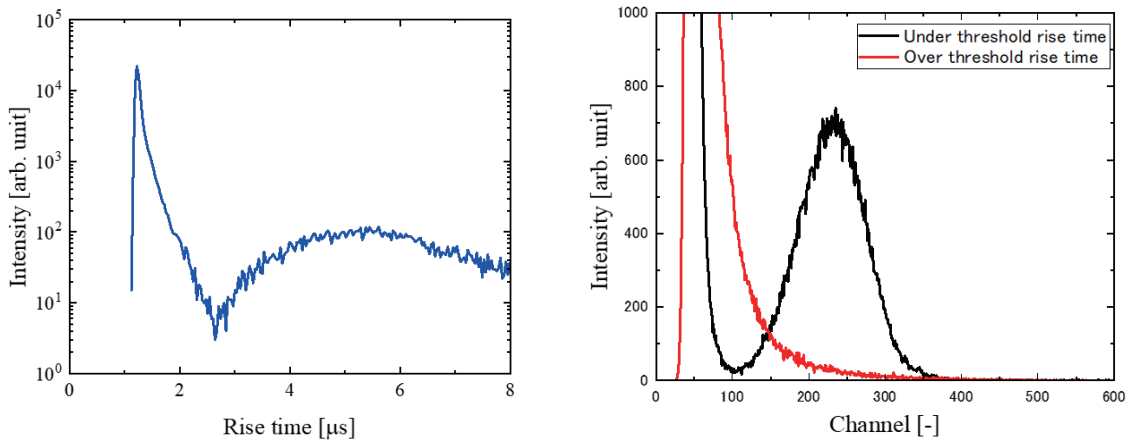

(a) (b)

Fig. 2. (Color online) (a) Rise-time histogram obtained using the energy channel greater than 125 ch at 573 K. (b) α-particle energy spectra below (black line) and above (red line) the threshold rise time of 2.5 μs at 573 K.

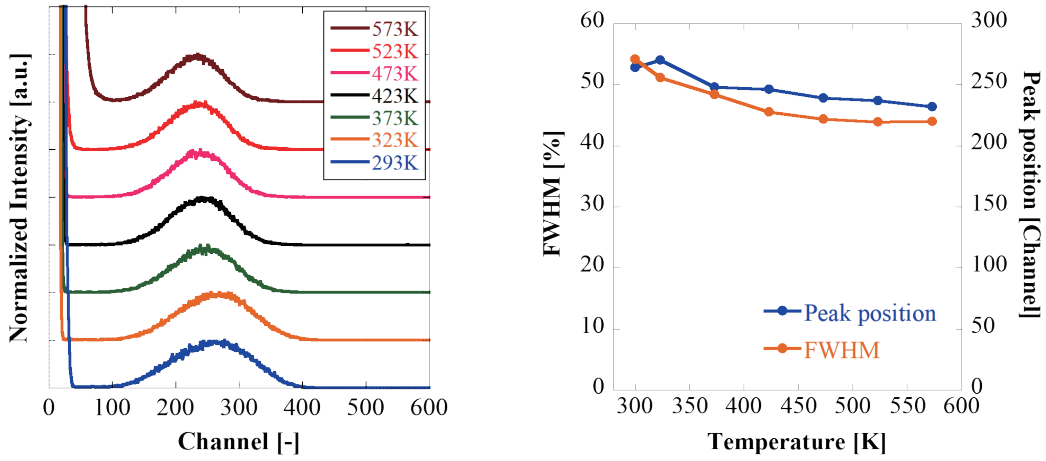

(a) (b)

Fig. 3. (Color online) (a) Energy spectra obtained using values under threshold rise time. (b) Peak position shift and FWHM values obtained from the energy spectra.

detection signal to a higher channel. On the other hand, the narrowing of the sensitive layer and depletion layer region due to the decrease in built-in potential with increasing temperature causes a shift of the detection signal to a lower channel.

As shown in Fig. 3(b), the FWHM of the α-particle peaks was also improved from 54% at 293 K to 40% at 573 K, indicating improved signal fluctuation. These results indicate that the wafer warpage due to rising temperature has been relaxed, improving crystallinity, and that in GaN-based detectors, when sapphire substrates are used, the wafer warpage due to the difference in thermal expansion coefficient has a significant effect on the detection characteristics.

To evaluate the improvement in carrier collection efficiency, the electron carrier mobility–lifetime product ($\mu_e\tau_e$) at 293 and 573 K were derived using Hecht's equation.[30] The $\mu_e\tau_e$ product was estimated by measuring the dependence of the energy spectrum on the applied voltage during the irradiation of α-particles. Figures 4(a) and 4(b) show the α-particle spectra of GaN obtained at various applied reverse bias voltages at 293 and 573 K, respectively. The peak position of α-particles shifted toward a higher-energy channel with increasing applied voltage at the two temperatures. Therefore, the carrier collection efficiency improved owing to the increased applied voltage. Figure 4(c) shows the dependence of the peak position in Fig. 4(a) on the applied voltage. The $\mu_e\tau_e$ product was derived using Hecht's equation as follows:

$$\mu_e\tau_e = \frac{D^2}{In\left(N_1 / N_2\right)}\left(\frac{1}{V_1} - \frac{1}{V_2}\right), \tag{1}$$

where N, V, and D are the measured peak centroid, the applied voltage, and the distance between the GaN diode electrodes, respectively. For a GaN detector, the n-GaN layer acts as a carrier-drift region owing to the high GaN resistance. Therefore, the $\mu_e\tau_e$ products were derived assuming D to be 30 mm. In particular, the preparation and evaluation of samples with different

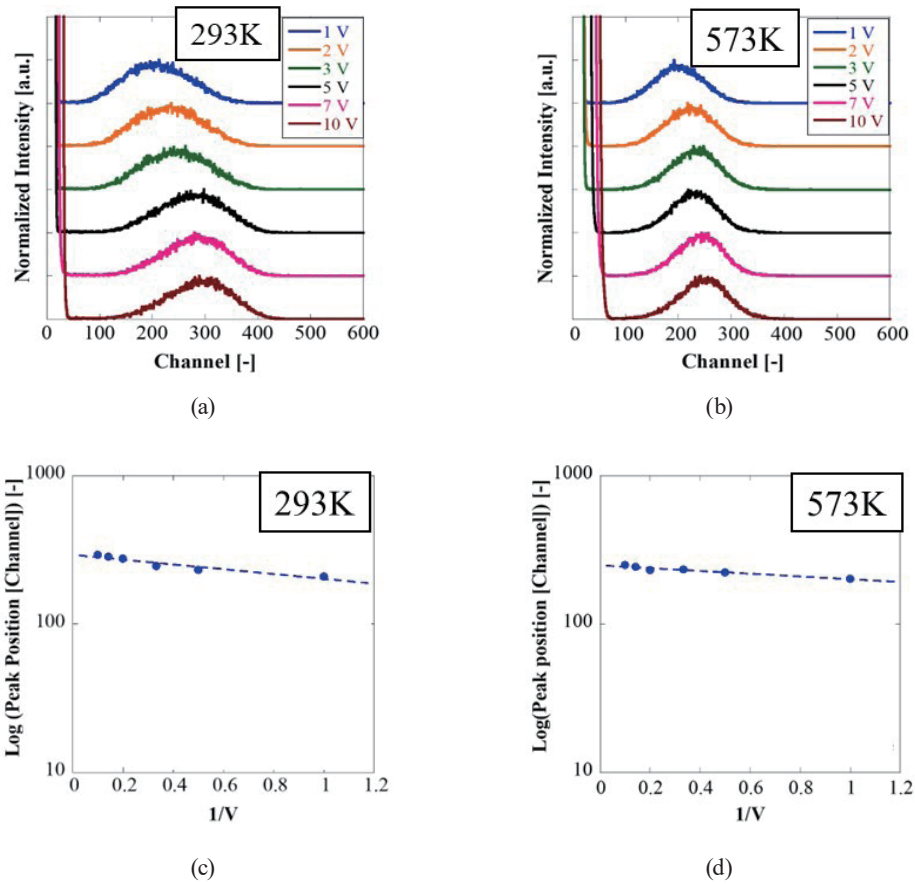

Fig. 4. (Color online) Applied voltage dependence of energy spectrum at (a) 293 K and (b) 573 K. Applied voltage dependence of peak position at (c) 293 and (d) 573 K.

film thicknesses are crucial. From this derivation, the $\mu_e\tau_e$ products of the GaN diode were 2.42 × 10^{-5} and 4.17 × 10^{-5} cm^2/V at 293 and 573 K, respectively. Hence, the carrier collection efficiency increased with temperature. Furthermore, $\mu_e\tau_e$ increased with temperature owing to the effect of improved crystallinity being greater than that of increased lattice scattering. The improved crystallinity is attributed to the recovery of crystal defects and the relaxation of compression strain on the sapphire substrate with increasing temperature.

These results indicate that the threshold rise time can be used to obtain a clear peak profile and satisfactorily evaluate the carrier collection efficiency at 573 K. Furthermore, a reduction in depletion layer thickness and an improvement in $\mu_e\tau_e$ product with increasing temperature were observed, although further analysis is required. Additionally, the mechanism behind the temperature dependence of crystal defects should be investigated using other analysis techniques.

4. Conclusions

We investigated GaN PIN diode detectors for α-particle detection at high temperatures. An increase in the region of noise components with increasing temperature was confirmed using a 2D histogram of the energy and rise time. The noise and detection signal components were distinguished by setting a suitable threshold rise time. Furthermore, the energy spectra plotted using the threshold confirmed the α-particle detection peak below 573 K. Hence, GaN PIN diode detectors can potentially detect radiation at high temperatures, indicating the possibility of high-temperature operation. Furthermore, the variations in peak profiles with increasing temperature confirmed the reduction in depletion layer thickness and the improvement in $\mu_e\tau_e$ product. Future research will focus on the in-depth investigation of these physical phenomena.

Acknowledgments

This work was partly supported by the Joint Research for Nuclear Safety R&D Center of Chubu Electric Power Corporation, the Joint Usage/Research Program of the Institute of Materials and Systems for Sustainability (IMaSS) at Nagoya University, MEXT Innovative Nuclear Research and Development Program Grant Number JPMXD0221459236, and JSPS KAKENHI Grant Nos. 16H03899 and 19H04394 from MEXT.

References

1 I. Akasaki and H. Amano: J. Electrochem. Soc. **141** (1994) 2266. https://dx.doi.org/10.1149/1.2055104
2 I. Akasaki and H. Amano: Jpn. J. Appl. Phys. **36** (1997) 5393. https://dx.doi.org/10.1143/JJAP.36.5393
3 T. Fujiwara, R. Yeluri, D. Denninghoff, J. Lu, S. Keller, J. S. Speck, S. P. DenBaars, and U. K. Mishra: Appl. Phys. Express **4** (2011) 096501. https://dx.doi.org/10.1143/APEX.4.096501
4 Y. Ando, K. Nagamatsu, M. Deki, N. Taoka, A. Tanaka, S. Nitta, Y. Honda, T. Nakamura, and H. Amano: Appl. Phys. Lett. **117** (2020) 242104. https://doi.org/10.1063/5.0028516
5 G. Xu, L. FengHua, L. Min, J. Yong, and L. Cheng: Sci. China Technol. Sci. **58** (2015) 1091. https://doi.org/10.1007/s11431-015-5802-7
6 M. Jeong, W. J. Jo, H. S. Kim, and J. H. Ha: Nucl. Instrum. Methods Phys. Res. A **784** (2015) 119. https://doi.org/10.1016/j.nima.2014.11.013
7 H. S. Kim, M. Jeong, Y. S. Kim, D. H. Lee, S. Y. Cho, and J. H. Ha: Nucl. Instrum. Methods Phys. Res. A **784** (2015)131. https://doi.org/10.1016/j.nima.2014.12.041
8 M. Niraula, D. Mochizuki, T. Aoki, Y. Tomita, T. Nihashi, and Y. Hatanaka: Nucl. Instrum. Methods phys. Res. A **436** (1999) 132. https://doi.org/10.1016/S0168-9002(99)00609-9
9 T. Terao, A. Koike, K. Takagi, H. Morii, T. Okunoyama, and T. Aoki: J. Instrum. **14** (2019) C06017. https://dx.doi.org/10.1088/1748-0221/14/06/C06017
10 H. Nakagawa, T. Terao, T. Masuzawa, T. Ito, A. Koike, H. Morii, and T. Aoki: Sens. Mater. **30** (2018) 1605. https://doi.org/10.18494/SAM.2018.1929
11 L. A. Kosyachenko, T. Aoki, C.P. Lambropoulos, V. A. Gnatyuk, S. V. Melnychuk, V. M. Sklyarchuk, E. V. Grushko, O. L. Maslyanchuk, and O. V. Sklyarchuk: J. Appl. Phys. **113** (2013) 054504. https://doi.org/10.1063/1.4790358
12 E. Kim, Y. Kim, A. E. Bolotnikov, R. B. James, and K. Kim: Nucl. Instrum. Methods phys. Res. A **923** (2019)51. https://doi.org/10.1016/j.nima.2019.01.064
13 N. R. Taylor, W. Kuang, M. Saeldijavash, P. Kandlakunta, Y. Zhang, and L. R. Cao: AIP Adv. **9** (2019) 095041. https://doi.org/10.1063/1.5119689
14 P. V. Raja, J. Akhtar, C. V. S. Rao, S. Vala, M. Abhangi, and N. V. L. N. Murty: Nucl. Instrum. Methods Phys. Res. A **869** (2017) 118. https://doi.org/10.1016/j.nima.2017.07.017
15 A. Datta, J. Fiala, P. Becla, and S. Motakef: APL Mater. **5** (2017) 106109. https://doi.org/10.1063/1.5001181

16 K. Hitomi, T. Onodera, S. Y. Kim, T. Shoji, and K. Ishii: Nucl. Instrum. Methods Phys. Res. A **747** (2014) 7. https://doi.org/10.1016/j.nima.2014.02.020
17 M. Nogami, K. Hitomi, T. Onodera, K. Matsumoto, K. Watanabe, A. Terakawa, and K Ishii: Nucl. Instrum. Methods Phys. Res. B **477** (2020) 43. https://doi.org/10.1016/j.nimb.2019.10.003
18 J. Wang, P. Mulligan, L Brillson, and L. R. Cao: Appl. Phys. Rev. **2** (2015) 031102. https://doi.org/10.1063/1.4929913
19 P. Mulligan, J. Wang, and L. Cao: Nucl. Instrum. Methods Phys. Res. A **719** (2013) 11. https://doi.org/10.1016/j.nima.2013.04.019
20 K. Atsumi, Y. Inoue, H. Mimura, T. Aoki, and T. Nakano: APL Mater. **2** (2014) 032106. https://doi.org/10.1063/1.4868176
21 T. Nakano, K. Mochizuki, T. Arikawa, H. Nakagawa, S. Usami, Y. Honda, H. Amano, A. Vogt, S. Schütt, M. Fieferle, K. Kojima, S.F. Chichibu, Y. Inoue, and T. Aoki: J. Appl. Phys. **130** (2021) 124501. https://doi.org/10.1063/5.0051053
22 M. Sugiura, M. Kushimoto, T. Mitsunari, K. Yamashita, Y. Honda, H. Amano, Y. Inoue, H. Mimura, T. Aoki, and T. Nakano: Jpn. J. Appl. Phys. **55** (2016) 05FJ02. http://doi.org/10.7567/JJAP.55.05FJ02
23 T. Nakano: JSAP Rev. **2023** (2023) 230201. https://doi.org/10.11470/jsaprev.230201
24 A. Takeyama, T. Matsuda, T. Yokoseki, S. Mitomo, K. Murata, T. Makino, S. Onoda, S. Okubo, Y. Tanaka, M Kandori, T. Yoshie, Y. Hijikata, and T. Ohshima: Jpn. J. Appl. Phys. **55** (2016) 104101. https://dx.doi.org/10.7567/JJAP.55.104101
25 M. Tsubota, J.H. Kaneko, D. Miyazaki, T. Shimaoka, K. Ueno, T. Tadokoro A. Chayahara, H. Watanabe, Y. Kato, S.Shikata, and H. Kuwabara: Nucl. Instrum. Methods Phys. Res. A **789** (2015) 50. https://doi.org/10.1016/j.nima.2015.04.002
26 W. S. Tan, M. J. Uren, P. W. Fry, P. A. Houston, R. S. Balmer, and T. Martin: Solid State Electron. **50** (2006) 511. https://doi.org/10.1016/j.sse.2006.02.008
27 V. C. Nguyen, K. Kim, and H. Kim: Micromachines **12** (2021) 400. https://doi.org/10.3390/mi12040400
28 G. Laffont, R. Cotillard, N. Roussel, R. Desmarchelier, and S. Rougeaul: Sensors **18** (2018) 1791. https://doi.org/10.3390/s18061791
29 T. Sato, Y. Iwamoto, S. Hashimoto, T. Ogawa, T. Furuta, S. Abe, T. Kai, P. E. Tsai, N. Matsuda, H. Iwase, N. Shigyo, L. Sihver, and K. Niita: J. Nucl. Sci. Technol. **55** (2018) 684. https://doi.org/10.1080/00223131.2017.1419890
30 K. Hecht: Z. Phys. **77** (1932) 235. https://doi.org/10.1007/BF01338917